FREEFEM++ FOR PIPETTE ASPIRATION

Raphael Lamprecht[1], Alexander Sutor[1]

[1] *Institute of Measurement and Sensor Technology, UMIT TIROL – Private University for Health Sciences and Health Technology, Eduard-Wallnoefer-Zentrum 1, Hall in Tirol, Austria*

This paper is a revised version of the authors' submitted manuscript that was peer-reviewed by at least two anonymous reviewers.

Abstract

Pipette aspiration is a widely used biomechanical technique for measuring the mechanical properties of cells and soft tissues. In this study, we present a computational model of pipette aspiration based on the finite element method, as implemented in FreeFem++. This model simulates tissue deformation under suction pressure, enabling us to analyze the system's frequency response. Our results demonstrate FreeFem++'s effectiveness in modelling complex biomechanical systems, providing insights into the viscoelastic properties of tissues under dynamic loading conditions.

Keywords: *pipette aspiration, finite element method, FreeFem++, biomechanics, frequency response*

1. Introduction

Pipette aspiration is a widely used technique in biomechanics for measuring the mechanical properties of cells and soft tissues. Deformation can be induced in the target tissue by applying controlled suction pressure through a pipette, and its response can be analyzed. This enables the elasticity, viscosity and viscoelasticity properties of soft tissues [1], [2] and phantoms [3] to be measured.

This method has been instrumental in advancing our understanding of tissue behavior under various physiological and pathological conditions. The mechanical properties of tissues are crucial for numerous biological processes, including voice production. Therefore, the pipette aspiration technique has been applied to investigate the viscoelastic properties of vocal fold tissues, which are essential for understanding voice production and disorders [4], [5], [6].

In pipette aspiration, the measured quantities are the applied pressure and the resulting tissue deformation (e.g., aspiration length), which are used to derive mechanical properties such as Young's modulus, shear modulus, and viscosity. Analytical formulations have been developed to relate pressure and deformation to these properties. These are typically based on the following assumptions: axisymmetry, simplified geometries (e.g., semi-infinite or finite-thickness layers), and linear elastic or linear viscoelastic material models [3], [7], [8]. However, interpretation under dynamic loading can be challenging due to geometric nonlinearity, viscoelastic dispersion, and potential inertial effects in biological tissues [9].

Computational modeling, particularly the finite element method (FEM), provides a framework to explore parameter regimes that are difficult to realize analytically [3]. FreeFem++ is open-source software that offers a flexible platform for implementing FEM simulations, making it a suitable tool for modeling complex biomechanical systems [10]. In this study, we present a computational model of pipette aspiration using FreeFem++ based on a viscoelastic constitutive law of the Kelvin-Voigt type [11]. We simulate tissue deformation under dynamic pressure and analyze the system's frequency response in the frequency domain of phonation from 0 Hz to 750 Hz to gain insights into viscoelastic properties under dynamic loading.

2. Methods

The measurement setup consists of a cylindrical pipette mounted on an optical coherence tomography system. The pipette is connected to a loudspeaker that generates a harmonic pressure signal, which excites the specimen inside the pipette. The resulting displacements are captured by an optical coherence tomography system, while the pressure inside the pipette is measured.

The details of the measurement setup and the specimen preparation are described in Lamprecht et al. [5]. The next section will focus on the computational model of pipette aspiration, as this is the focus of this study.

2.1. Governing equations

The material is assumed to be viscoelastic of the Kelvin-Voigt type, which can be described by

Corresponding author: *raphael.lamprecht@umit-tirol.at.*

$$
\begin{cases}
\big[\nabla(\lambda\,\nabla\cdot\mathbf{u})+\nabla\cdot(2\mu\,\varepsilon(\mathbf{u}))\big]+i\omega\big[\nabla(\zeta\,\nabla\cdot\mathbf{u})+\nabla\cdot(2\eta\,\varepsilon(\mathbf{u}))\big]+\rho\omega^2\mathbf{u}=0, & \text{in } \Omega,\\
\mathbf{u}=\mathbf{f} & \text{on } \Gamma_D,\\
\partial_{\mathbf{n}}\mathbf{u}:=\big[\lambda\,\nabla\cdot\mathbf{u}+2\mu\,\varepsilon(\mathbf{u})\big]\nu+i\omega\big[\zeta\,\nabla\cdot\mathbf{u}+2\eta\,\varepsilon(\mathbf{u})\big]\,\mathbf{n}=0, & \text{on } \Gamma_N,\\
\partial_{\mathbf{n}}\mathbf{u}=p_0\,\mathbf{n}, & \text{on } \Gamma_P,
\end{cases}
\tag{1}
$$

with $\varepsilon(\mathbf{u})$ being the strain tensor, ω the angular frequency, ρ the density, $\mathbf{u}$ the displacement vector. The boundary Γ_N is traction free, Γ_D is a displacement boundary, whereas at Γ_P a pressure p_0 is applied, with the $\mathbf{n}$ being the outward unit normal vector to $\partial\Gamma$. The physical interpretation of the model in Eq. (1) is as follows: the first bracket describes elastic restoring forces, the second bracket describes viscous dissipation (scaled by $i\omega$ in the frequency domain), and the term $\rho\omega^2\mathbf{u}$ represents inertia. Boundary conditions prescribe a mixture of displacement ($\mathbf{u}=\mathbf{f}$ on Γ_D), traction-free surfaces ($\partial_{\mathbf{n}}\mathbf{u}=0$ on Γ_N), and pressure loading ($\partial_{\mathbf{n}}\mathbf{u}=p_0\mathbf{n}$ on Γ_P). The existence, uniqueness, and exponential decay of solutions to the mixed-boundary problem for anisotropic viscoelastic materials governed have been shown in Jiang et al. [11]. The material parameters are generally complex-valued: the shear modulus is given by $\mu^*=\mu+i\omega\eta$, where μ is the storage modulus and η is the loss modulus, representing the dissipative effects in the viscoelastic medium. Similarly, the compression modulus and compression viscosity are given by λ and ζ, respectively [11], [12]. The material parameters μ and λ are related to the Young's modulus E and the Poisson's ratio ν by $\mu=\frac{E}{2(1+\nu)}$ and $\lambda=\frac{E\nu}{(1+\nu)(1-2\nu)}$.

Reported values for the Poisson's ratio of vocal fold tissue range from 0.3 to 0.5, with the upper bound 0.5 representing the incompressible limit. The silicone rubber employed in this study exhibits a Poisson's ratio of 0.499 [13], closely approximating this limit. Consequently, at low frequencies, Hz to kHz, the third term in Eq. (1), which involves the compressional viscosity parameter ζ, may be neglected under the quasi-incompressible assumption [14], [15], [16]. On the other hand, in the first term, the large magnitude of λ is counterbalanced by the correspondingly small magnitude of $\nabla(\nabla\cdot\mathbf{u})$ and consequently cannot be neglected [14].

The harmonic analysis is implemented in FreeFem++ [10], whereby the variational form of Eq. (1) for the *stationary viscoelasticity equation* is given by

$$
\begin{aligned}
&\int_\Omega 2\mu\,\varepsilon(\mathbf{u}):\varepsilon(\mathbf{v})+\int_\Omega \lambda\,(\nabla\cdot\mathbf{u})(\nabla\cdot\mathbf{v})\\
&+i\omega\int_\Omega 2\eta\,\varepsilon(\mathbf{u}):\varepsilon(\mathbf{v})-\int_\Omega \rho\,\omega^2\,\mathbf{u}\cdot\mathbf{v}\\
&=\int_{\Gamma_P}(p_0\cdot\mathbf{n})\cdot\mathbf{v}
\end{aligned}
\tag{2}
$$

using the test function $\mathbf{v}$ [11].

2.2. Geometry & boundary conditions

The geometry of the problem is depicted in Fig. 1. The domain Ω is a cylindrical region representing the silicone rubber specimen, with the boundaries Γ_P and Γ_D corresponding to the pressure and displacement boundary conditions, respectively. The geometric parameters are as follows: pipette inner radius $r_i=1.5\,\mathrm{mm}$, pipette outer radius $r_o=2.5\,\mathrm{mm}$, specimen height $h_s=10.0\,\mathrm{mm}$, and specimen radius $r_s=50.0\,\mathrm{mm}$.
The geometry of the specimen is axisymmetric, and the problem is formulated in cylindrical coordinates (r,θ,z), with the axis of symmetry aligned with the z-axis. Using the symmetry of the problem, the computational domain is reduced to a two-dimensional region in the $r-z$ plane, where r is the radial coordinate and z is the axial coordinate.

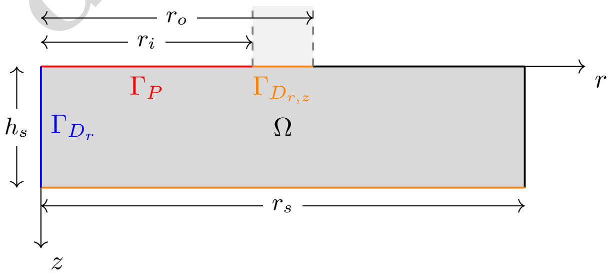

Figure 1: Boundary conditions for the harmonic model. Different colors represent specific boundary conditions: the red line corresponds to the pressure boundary condition, Γ_P; the orange line indicates the displacement boundary, $\Gamma_{D_{r,z}}$, where displacements in both the r and z directions are constrained to zero. The blue line marks the symmetry axis, Γ_{D_r}, along which radial displacement vanishes. The black line outlines the outer specimen boundary, which is subject to a traction-free condition. The gray dashed line illustrates the pipette, which is excluded from the computational domain.

The displacement at Γ_D is prescribed to be zero, representing a clamped boundary condition. The pressure p_0 at Γ_P is applied uniformly across the boundary.

2.3. Benchmark models

Aoki's approximation derives Young's modulus from the applied pressure, the central displacement, and the pipette inner radius, scaled by a geometry-dependent constant obtained from linear, axisymmetric FEM of an isotropic, incompressible, homogeneous specimen with experimental verification. For the present pipette with an outer-to-inner radius ratio of 1.67, the constant is about 1.01, and the influence of specimen dimensions is considered minor and neglected [7].

Theret's approximation models micropipette aspiration with an axisymmetric elastic-foundation boundary condition that enforces zero normal surface displacement for an incompressible material. The modulus is obtained from the same measurable quantities as above, multiplied by a geometry-dependent factor that is approximately 2.02 for the current pipette [8]. Zhang's approximation uses a Neo-Hookean hyperelastic framework to estimate the modulus from pressure and displacement normalized by the pipette inner radius. It typically distinguishes linear and nonlinear regimes; here, the linear small-deformation expression is employed [3].

3. Model validation

The default parameters, shown in Table 1, were used to validate the model.

Table 1: Default parameters for the model validation.

Parameter	Value
Elastic modulus E	10 kPa
Poisson ratio ν	0.499
Loss modulus η	1 Pa s
Compressional viscosity ζ	neglected
Density ρ	$1000\,\mathrm{kg\,m^{-3}}$
Frequency range f	0 Hz to 700 Hz
Pressure amplitude p	25 Pa

A mesh study was carried out to determine the optimal mesh size for the simulation. The mesh was refined until the relative error of the displacement field was below the expected deviation of $\pm 1\,\%$. The final model uses a remeshing strategy, which is based on an exponential growth of the element size from the pipette center, see Fig. 2. Therefore the computational time is reduced significantly, without losing accuracy.

3.1. Displacement field

Fig. 2 shows the displacement field at an excitation frequency of 291 Hz.The maximum displacement occurs at the center of the pipette, consistent with the applied boundary conditions and the axisymmetric loading. The displacement magnitude decreases radially outward from the center, which is consistent with the expected axisymmetric deformation pattern for a pipette aspiration setup in which the applied suction is concentrated within a region near twice the inner radius of the pipette and the surrounding region provides constraint [7].

3.2. Parameter study

The material parameters, the Young's modulus E, the Poisson's ratio ν, the loss modulus η and the density ρ, were varied to determine the influence on

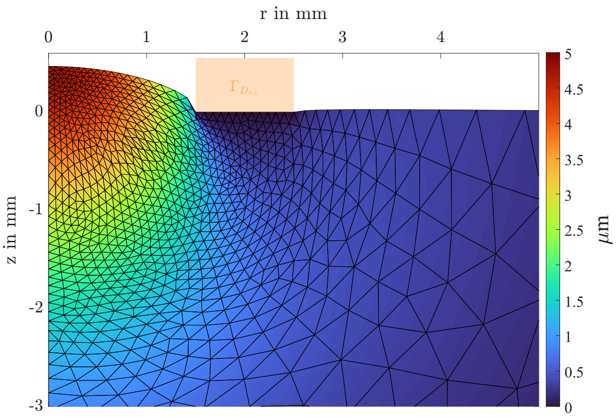

Figure 2: The displacement field for an excitation frequency of 291 Hz. The color shows the magnitude of the displacement, and the deformation of the mesh is scaled by a factor of 100 for visualization. The boundary $\Gamma_{D_{r,z}}$, the contact between the pipette and the specimen is, indicated as orange region.

the central displacement magnitude and phase. The results are shown in Fig. 3, with the displacement magnitude and phase shown in the upper and lower panel, respectively. The damped resonant frequency of the system is indicated at the maximum magnitude response, while the undamped resonant frequency is identified at $-90°$ in the phase response [17].

It can be seen in Fig. 3a that the Young's modulus E has a significant effect on the displacement magnitude, with the damped resonant frequency being shifted to higher frequencies and the displacement decreasing as the Young's modulus increases. The same trend is observed for the phase response, with the undamped resonant frequency shifting to higher frequencies as the Young's modulus increases.

The viscosity parameter η influences the displacement magnitude, as shown in Fig. 3b. The viscosity has no influence on the quasi-static case at 0 Hz, which is a purely elastic static deformation. As η increases, the maximum displacement decreases, and the corresponding damped resonant frequency shifts to lower values. At high viscosity values, the maximum displacement is observed at 0 Hz. The phase response indicates that the undamped resonant frequency is only slightly affected by the viscosity parameter η.

The Poisson's ratio ν barely influences the displacement magnitude, as shown in Fig. 3c, with the damped resonant frequency shifting only slightly to higher values as ν increases. In contrast, the undamped resonant frequency shifts to lower values with increasing ν.

Fig. 3d shows that the density ρ has little effect on the displacement magnitude and the damped resonant frequency. However, as the density increases, the damped resonant frequency shifts to lower values, while the displacement magnitude increases. A similar trend is observed for the phase response, with the undamped resonant frequency shifting to lower frequencies as the density increases.

3.3. Pressure amplitude

The displacement magnitude increases linearly with the pressure amplitude, as expected from the linear relationship between pressure and displacement in Eq. (2). The resonant frequencies and the phase response are unaffected by the pressure amplitude, as both are determined by the material properties, rather than the magnitude of the applied pressure.

3.4. Measurement point

The measured displacement decreases with increasing radial offset of the measurement point from the pipette center, consistent with the imposed boundary conditions and the expected deformation pattern, as shown in Fig. 4. The phase response likewise depends on the measurement location due to the applied boundary conditions. An offset of 0.1 mm results in a relative error of approximately 0.5 % at the damped resonant frequency of 295 Hz, whereas at 0.5 mm the error increases to nearly 7.5 %. Here "relative error" is defined with respect to the on-axis (center) response predicted by the model. In practice, however, an offset of only 0.1 mm remains sufficiently accurate.

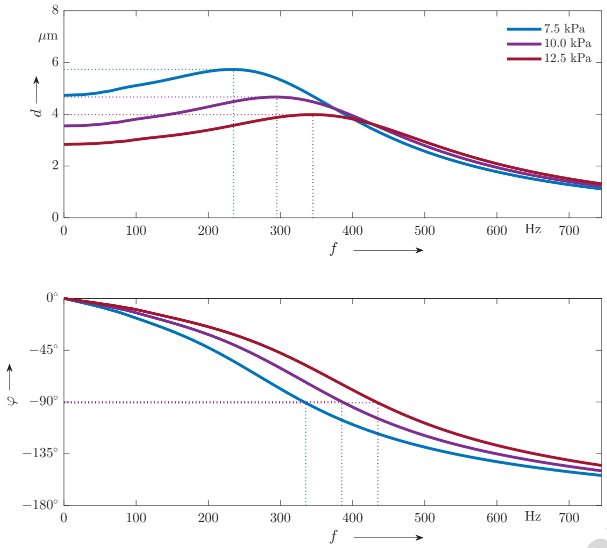

(a) Variation of the Young's modulus E.

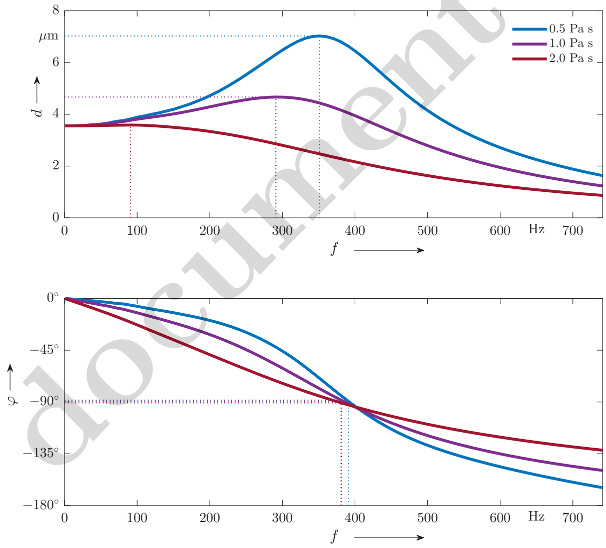

(b) Variation of the viscosity parameter η.

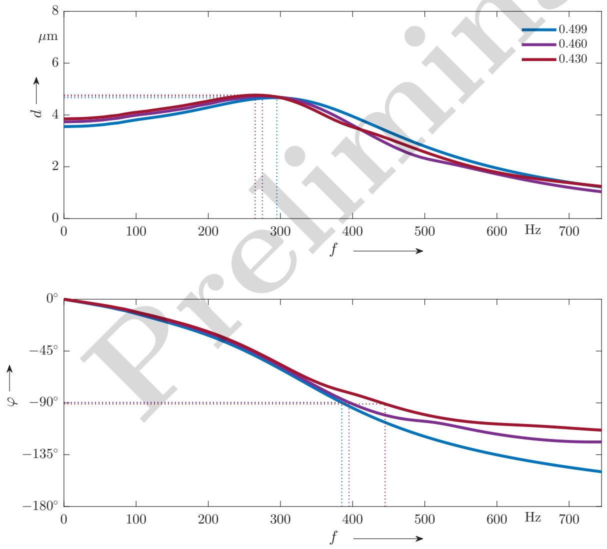

(c) Variation of the Poisson's ratio ν.

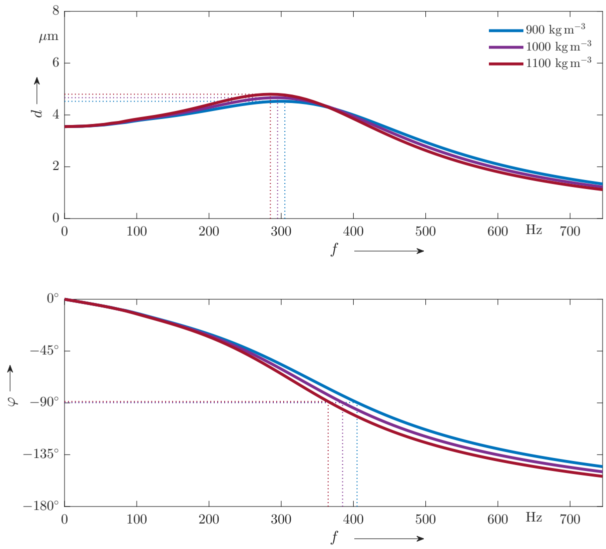

(d) Variation of the density ρ.

Figure 3: Complex frequency response (magnitude and phase) of the pipette over 0 Hz to 700 Hz for variations in material parameter: Young's modulus E, viscosity parameter η, Poisson ratio ν, and density ρ. The upper panel shows the magnitude response of the displacement d at the pipette center and the damped resonant frequency of the system is indicated. The lower panel shows the phase φ, where the undamped resonant frequency is identified at $-90°$.

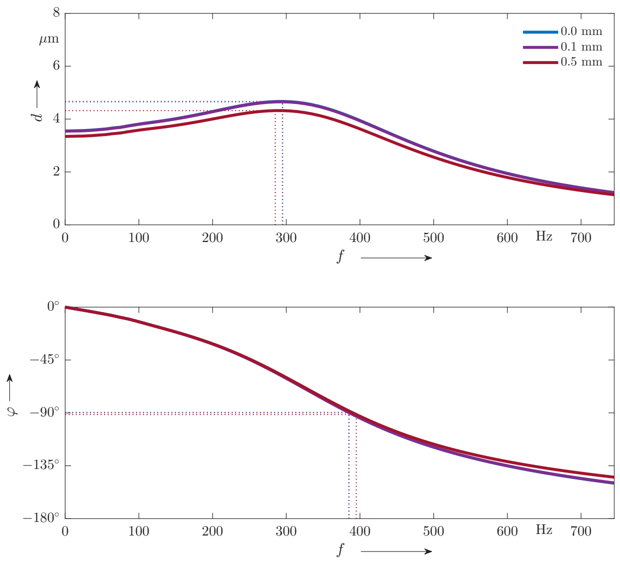

Figure 4: Effect of the measurement-point offset in the range of 0 mm to 0.5 mm from the pipette center on the measured displacement magnitude and phase.

3.5. Comparison to established methods

In the static case with $f = 0\,\mathrm{s}^{-1}$, the differential equation Eq. (2) reduces to the elastic formulation, neglecting the viscous and inertia effects. Therefore, only the Young's modulus, the Poisson's ratio and the pressure amplitude have an influence on the displacement field. The presented model, will be compared to the approximations of Aoki, Theret and Zhang.

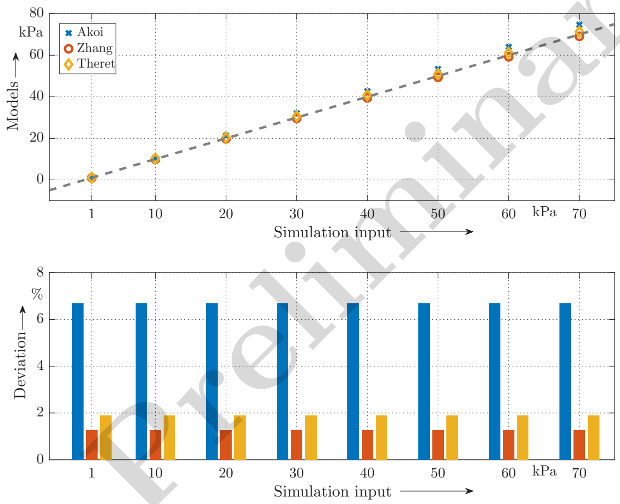

Figure 5: Comparison of the literature models with the numerical simulation for the Young's modulus at 0 Hz. The dashed line represents the input Young's modulus of the simulation and therefore the expected value.

The comparison of the approximations with the numerical simulation for the Young's modulus is shown in Fig. 5. The approximations show a good agreement with the numerical simulation, with Theret's approximation ($D_{\max} = 1.27\,\%$) and Zhang's linear approximation ($D_{\max} = 1.89\,\%$) showing lowest relative deviation $D_{\max}$. The approximation of Aoki shows a worse agreement, with a maximum deviation of $D_{\max} = 6.7\,\%$.

The elastic portion of the model is therefore consistent with the literature, and the approximations show a good agreement with the numerical simulation in the static case. However, in the dynamic case, the approximations deviate significantly from the numerical simulation, as they do not account for the viscous effects, which become more significant at higher frequencies, as shown in Fig. 6.

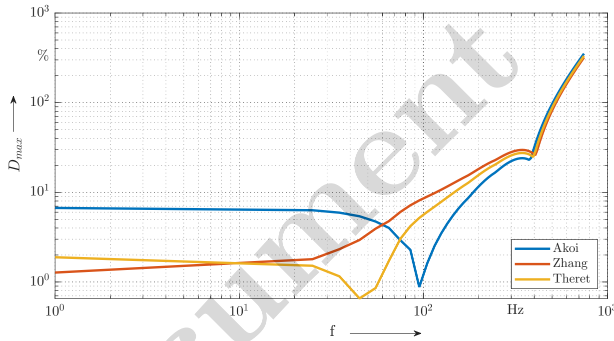

Figure 6: The maximum deviation of the approximations from the numerical simulation for the Young's modulus at different frequencies, where the deviation is given in percentage of the input Young's modulus of the simulation.

4. Discussion

In this study, we presented a computational model of pipette aspiration using FreeFem++. The model was based on a viscoelastic constitutive law of the Kelvin-Voigt type and simulated tissue deformation under dynamic pressure. We analyzed the system's frequency response within the frequency domain of phonation from 0 Hz to 750 Hz to gain insights into viscoelastic properties under dynamic loading.

To ensure interpretability and reproducibility, we performed mesh- and frequency-step convergence studies and benchmarked the model against established solutions in the quasi-static, linear elastic limit. Our results demonstrated that FreeFem++ can reproduce aspiration responses and resolve frequency-dependent behavior within the targeted range. This provides a computational framework for future studies on tissue mechanics. We also delineated the model's limitations, most notably the assumptions of linear viscoelasticity and the omission of air–structure interaction within the pipette lumen. Because the pressure is prescribed from measurement rather than obtained from a coupled air-domain model, the simulation does not resolve the bidirectional interaction between specimen motion and the air column in the pipette. Consequently, it omits additional aerodynamic loading associated with lumen air motion, including viscous losses, inertial phase delays, and possible acoustic resonances of the

pipette air column. Any frequency dependence predicted by the model should therefore be attributed primarily to the viscoelastic response of the solid, although some pneumatic effects may still be embedded implicitly in the prescribed pressure boundary condition. Accordingly, the model is most applicable to small-amplitude, approximately harmonic deformations, where the solid response is expected to dominate. Its predictive value is more limited for large aspiration amplitudes, transient or strongly non-sinusoidal loading, higher-frequency excitation, or geometries in which air-column dynamics become comparable to the structural response.
The data produced in this process will be used as a basis for future validation against experimental data and to train machine learning models for parameter estimation. The model's ability to capture the frequency-dependent behavior of tissues under dynamic loading conditions is particularly relevant for applications in voice production, where the viscoelastic properties of vocal fold tissues play a crucial role.

References

[1] Y. Ding, G.-F. Wang, X.-Q. Feng, and S.-W. Yu, "Micropipette aspiration method for characterizing biological materials with surface energy," *J. Biomech.*, vol. 80, pp. 32–36, Oct. 2018. DOI: 10.1016/j.jbiomech.2018.08.020

[2] T. Boudou, J. Ohayon, Y. Arntz, G. Finet, C. Picart, and P. Tracqui, "An extended modeling of the micropipette aspiration experiment for the characterization of the young's modulus and poisson's ratio of adherent thin biological samples: Numerical and experimental studies," *J. Biomech.*, vol. 39, no. 9, pp. 1677–85, Jan. 2006. DOI: 10.1016/j.jbiomech.2005.04.026

[3] M.-G. Zhang, Y.-P. Cao, G.-Y. Li, and X.-Q. Feng, "Spherical indentation method for determining the constitutive parameters of hyperelastic soft materials," *Biomech. Model. Mechanobiol.*, vol. 13, no. 1, pp. 1–11, Jan. 2014. DOI: 10.1007/s10237-013-0481-4

[4] F. Scheible, R. Lamprecht, M. Semmler, and A. Sutor, "Dynamic biomechanical analysis of vocal folds using pipette aspiration technique," *Sens.*, vol. 21, no. 9, p. 2923, Jan. 2021. DOI: 10.3390/s21092923

[5] R. Lamprecht, F. Scheible, and A. Sutor, "Combination of pipette aspiration and OCT: A novel method for frequency-dependent elasticity assessment of silicone tissue phantoms," *Meas.: Sens.*, p. 101 653, Jan. 2025. DOI: 10.1016/j.measen.2024.101653

[6] R. Lamprecht, M. Semmler, and A. Sutor, "Dynamic OCT pipette aspiration technique for frequency-dependent biomechanical characterization of vocal folds," *Measurement*, vol. 264, p. 120 164, Mar. 2026. DOI: 10.1016/j.measurement.2025.120164

[7] T. Aoki, T. Ohashi, T. Matsumoto, and M. Sato, "The pipette aspiration applied to the local stiffness measurement of soft tissues," *Ann. Biomed. Eng.*, vol. 25, no. 3, pp. 581–7, Jan. 1997. DOI: 10.1007/BF02684197

[8] D. P. Theret, M. J. Levesque, M. Sato, R. M. Nerem, and L. T. Wheeler, "The application of a homogeneous half-space model in the analysis of endothelial cell micropipette measurements," *J. Biomech. Eng.*, vol. 110, no. 3, pp. 190–199, Aug. 1988. DOI: 10.1115/1.3108430

[9] S. Zörner, M. Kaltenbacher, R. Lerch, A. Sutor, and M. Döllinger, "Measurement of the elasticity modulus of soft tissues," *J. Biomech.*, vol. 43, no. 8, pp. 1540–1545, May 2010. DOI: 10.1016/j.jbiomech.2010.01.035

[10] F. Hecht, "New development in freefem++," *J. Numer. Math.*, vol. 20, no. 3-4, pp. 251–266, Dec. 2012. DOI: 10.1515/jnum-2012-0013

[11] Y. Jiang, H. Fujiwara, and G. Nakamura, "Approximate steady state models for magnetic resonance elastography," *SIAM J. Appl. Math.*, vol. 71, no. 6, pp. 1965–1989, Jan. 2011. DOI: 10.1137/100781882

[12] H. Ammari, J. K. Seo, and L. Zhou, "Viscoelastic modulus reconstruction using time harmonic vibrations," *Math. Modell. Anal.*, vol. 20, no. 6, pp. 836–851, Nov. 2015. DOI: 10.3846/13926292.2015.1117531

[13] S. Weiss, A. Sutor, J. Ilg, S. J. Rupitsch, and R. Lerch, "Measurement and analysis of the material properties and oscillation characteristics of synthetic vocal folds," *Acta Acust. united Acust.*, vol. 102, no. 2, pp. 214–229, Jan. 2016. DOI: 10.3813/AAA.918938

[14] R. Sinkus et al., "Imaging anisotropic and viscous properties of breast tissue by magnetic resonance-elastography," *Magn. Reson. Med.*, vol. 53, no. 2, pp. 372–387, Feb. 2005. DOI: 10.1002/mrm.20355

[15] L. E. Kinsler, Ed., *Fundamentals of Acoustics*, 3. New York: Wiley, 1982, ISBN: 978-0-471-02933-5.

[16] R. Sinkus, M. Tanter, T. Xydeas, S. Catheline, J. Bercoff, and M. Fink, "Viscoelastic shear properties of in vivo breast lesions measured by MR elastography," *Magn. Reson. Imaging*, vol. 23, no. 2, pp. 159–65, Jan. 2005. DOI: 10.1016/j.mri.2004.11.060

[17] R. W. Chan and M. L. Rodriguez, "A simple-shear rheometer for linear viscoelastic characterization of vocal fold tissues at phonatory frequencies," *J. Acoust. Soc. Am.*, vol. 124, no. 2, pp. 1207–1219, Aug. 2008. DOI: 10.1121/1.2946715